Long-range Signaling by Phosphoprotein Waves Arising from Bistability in Protein Kinase Cascades

Nick I. Markevich[*], Mikhail A. Tsyganov[*], Jan B. Hoek & Boris N. Kholodenko[#]

Department of Pathology, Anatomy and Cell Biology, Thomas Jefferson University, 1020 Locust St., Philadelphia, PA 19107, USA.

[*]*These authors contributed equally to this work*

Supplementary Information

Kinetic analysis of MAPK cascade in time and space. Our MAPK cascade models resemble models developed previously by us and others (Asthagiri and Lauffenburger, 2001; Huang and Ferrell, 1996; Kholodenko, 2000; Markevich et al., 2004a), but explicitly incorporate heterogeneous spatial distribution of activated kinases (Kholodenko, 2002; Maly et al., 2004). We initially consider a spherical cell of radius L = 15 μm with a nucleus of radius Q = 6 μm for illustrative purposes (Fig. S1).

Supplementary Fig.S1

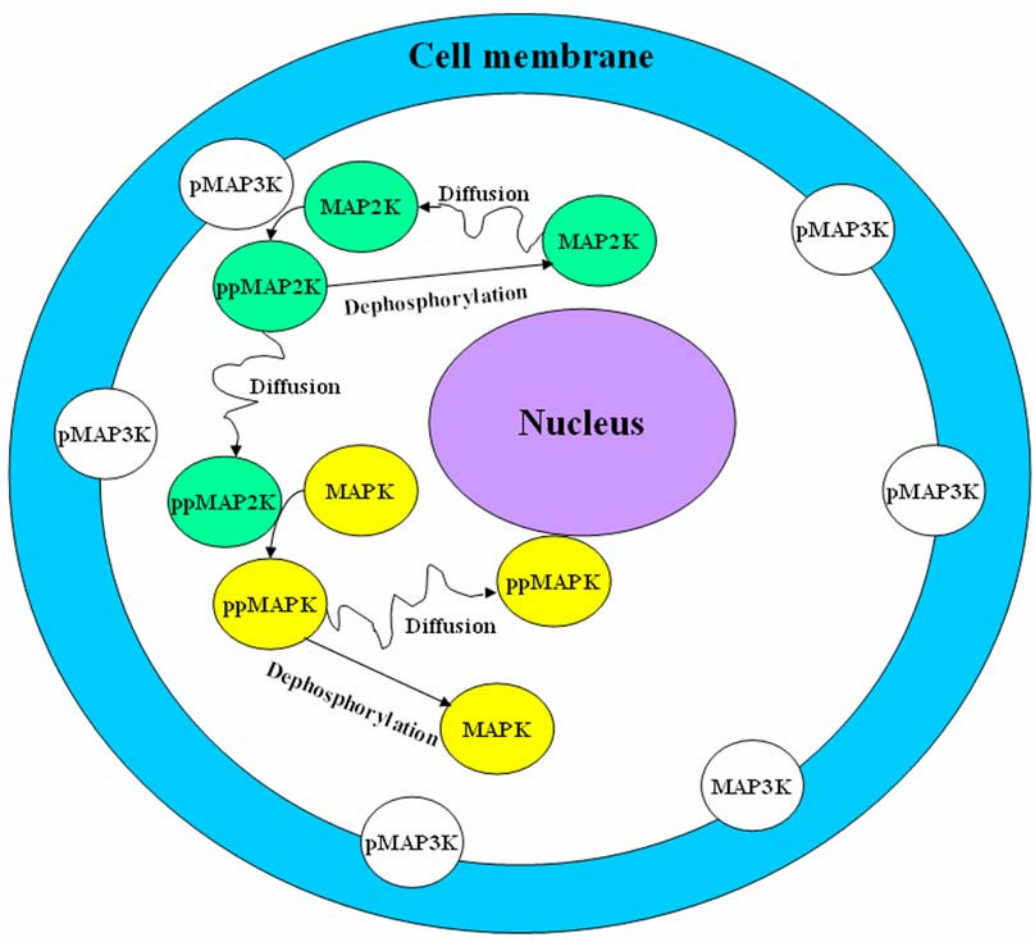

Fig. S1. Spatial separation of signaling reactions in MAPK cascades. MAP3K and MAP2K are phosphorylated and dephosphorylated at the PM. In addition, MAP2K is dephosphorylated by cytosolic phosphatases, while the phosphorylated MAP2K forms diffuse in the cytoplasm. MAPK is phosphorylated and dephosphorylated in the cytoplasm. Active MAP2K and MAPK drift to the nucleus.

Supplementary Fig.S2

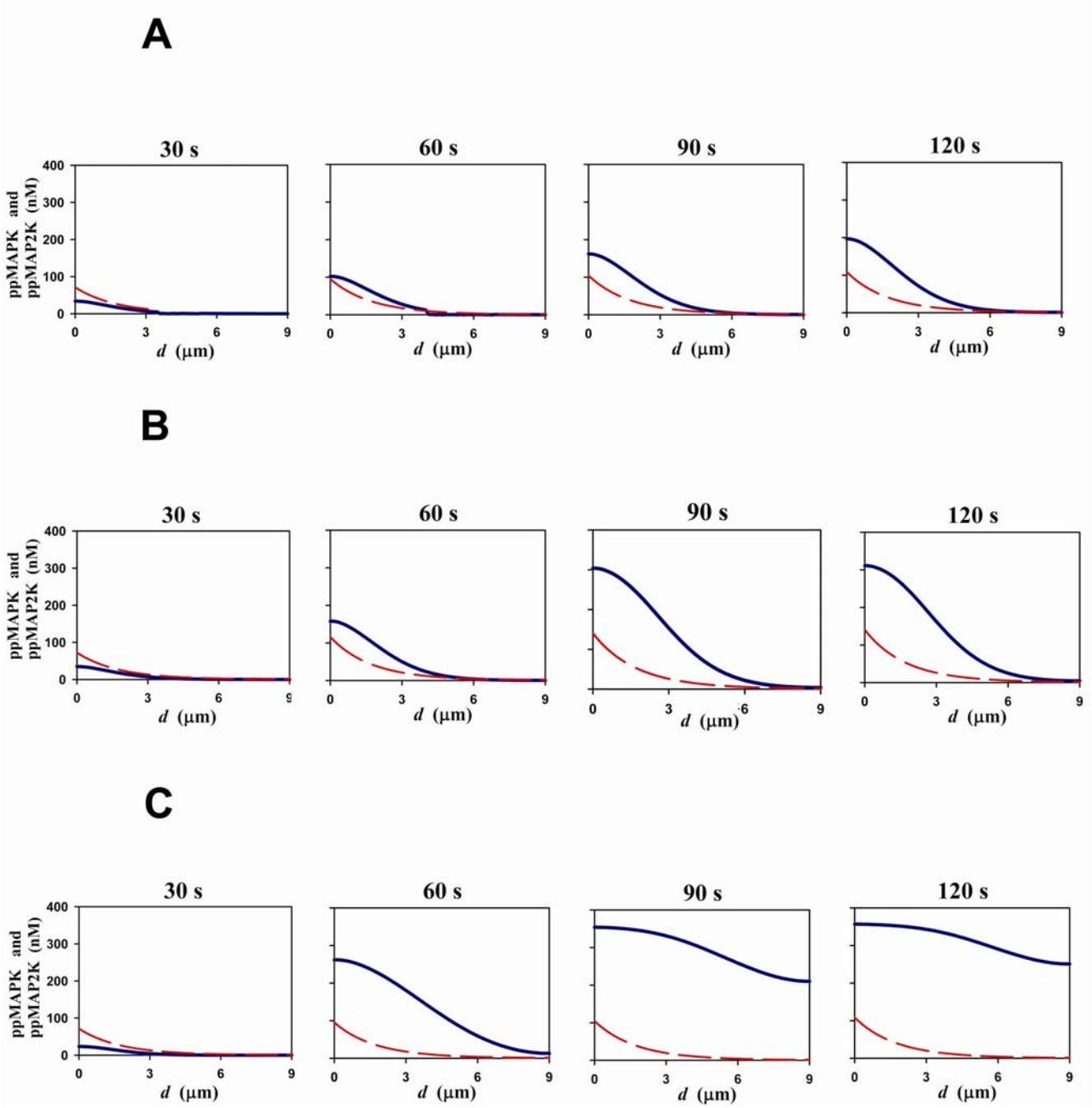

Fig. S2. Spatial propagation of MAPK activation in response to sustained Ras/MAP3K stimulation: dependence on the feedback design and input-output relationships. (A-C) Dynamics of the ppMAPK spatial profiles following the onset of sustained Ras/MAP3K activation for three different feedback designs that result in the stimulus-response dependencies shown in Fig. 1A-C of the main text. Solid (blue) and dashed (red) lines correspond to [ppMAPK] and [ppMAP2K], respectively. *d* is the distance from the cell membrane. [Ras-GTP] = 30 nM. The differential equations and kinetic parameters are given in Tables I-III of the main text.

Supplementary Fig.S3

Activation of cell surface receptors is usually transient and results in a transient rather than sustained activation of MAP3K at the cell membrane. Various mammalian cells stimulated with growth factors, cytokines or other ligands typically demonstrate a transient Ras activation with 3 – 20-fold increase in the peak Ras-GTP level over basal activity ((Chiloeches et al., 1999)). The transient Ras-GTP signal is detected on the time scale of minutes, although a low stationary activity that is higher than the basal level can be maintained for longer times (reviewed in (Markevich et al., 2004b)). Based on mammalian cell data, the Ras-GTP concentration pattern is simulated in the model as a function of time (insert to Fig. S3A), which increases from the zero level in a sigmoidal manner, rapidly reaches a peak value and then decreases to a low sustained level on the time scale of minutes. Fig. S3A illustrates that when the Ras-GTP level (the input signal for the MAPK cascade) is transient, then bisphosphorylated MAPK near the nucleus is also transient, except when the remaining, quasi-stationary Ras-GTP signal is sufficiently high ($\geq$20 nM) to elicit a sustained MAPK activation. Hysteresis in the input-output relations for MAPK cascade implies the existence of two different thresholds, high for full activation and a lower threshold for deactivation (Figs. 1B and 1C of the main text). Owing to this kind of biological "memory", the active MAPK fraction at the nuclear boundary depends not only on a stationary input level, but also on the amplitude and rate of the initial increase in the input signal. As a result, to induce MAPK activation close to the nucleus the amplitude of a sustained signal (Ras-GTP) should be greater than the remaining, quasi-stationary Ras-GTP level that is maintained after a high peak level (cf. Fig. S3A and Fig. 1E of the main text).

We can see that during transient MAPK signaling, the peak MAPK level near the nucleus is similar to the level near the cell surface, only when the relay of the phosphorylated signal is enhanced by bistability in the MAPK cycle in the cytoplasm (Fig. S3A). Importantly, calculations also suggest that even a marked decrease in the phosphorylated MAPK fraction seen in the perinuclear area may not be readily detectable when ppMAPK is averaged over the whole cell (Fig. S3B), as it occurs in the experiments that use usual western blot protocols. Indeed, when the concentration profile is integrated over the cell volume, the contribution of the areas near the cell surface with high bisphosphorylated MAPK is much greater than that of the areas deep into the cell interior (because the volume of a thin layer at the distance d from the cell center is proportional to $4\pi d^2$). Fig. S4 further confirms that bistability in the MAPK cycle facilitates the signal propagation and illustrates how MAPK activation spreads in the space and eventually vanishes following a transient stimulation of Ras at the membrane.

Supplementary Fig.S3

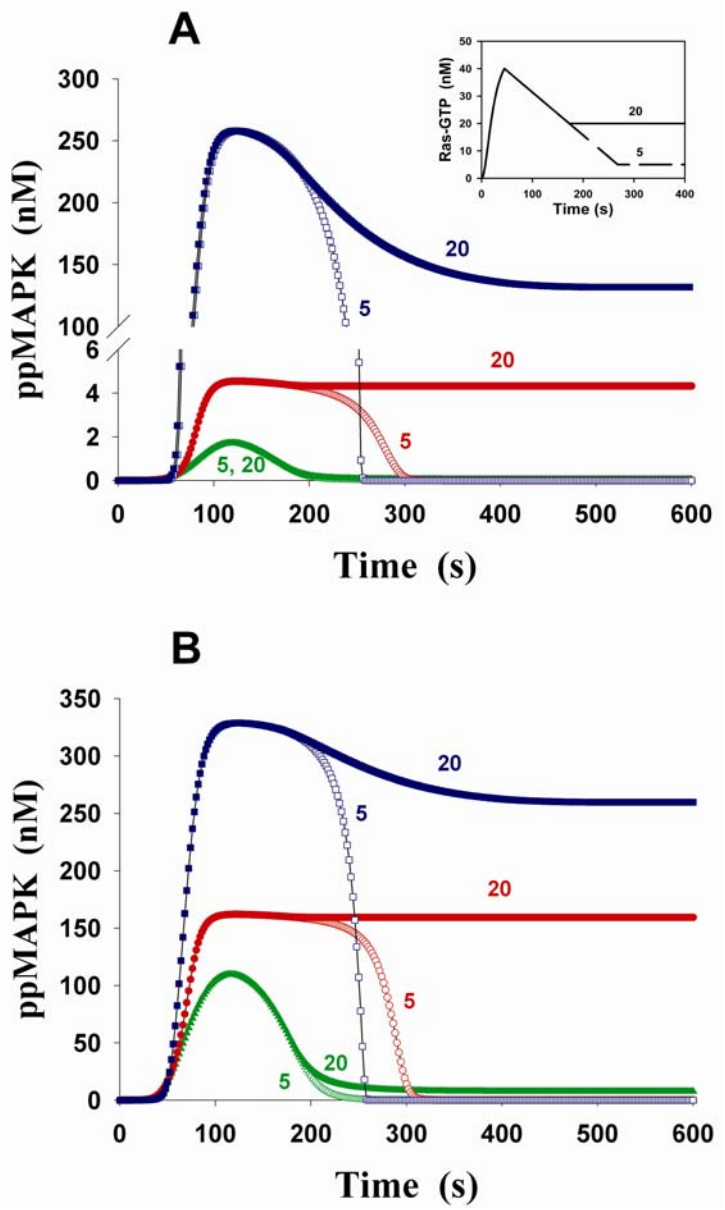

Fig. S3. Activation of MAPK by transient Ras stimulation. (A) Time course of active MAPK concentration close to the nucleus and **(B)** bulk averaged concentration of active MAPK**.** For three different kinetic mechanisms shown in Fig. 1A-C of the main text, MAPK activation profiles are presented by triangles (green) for ultrasensitive response, by circles (red) for a long positive feedback loop from MAPK to Ras/MAP3K and by squares (blue) for the bistable ERK cycle. The time course of Ras-GTP was simulated *in silico* as the following function of time (Markevich et al., 2004b): for the time interval, $0 < t < 45$ s, Ras-GTP $(t) = at^2/(b^2 + t^2)$, a = 50 nM, b = 22.5 s. For $t > 45$ s, Ras-GTP$(t) = c\cdot(T - t)$, $c = 0.157$ nM$\cdot$s^{-1}, T = 300 s. Ras-GTP descends down to a sustained level of: 20 nM - filled triangles, circles and squares (▲, ●, ■), 5 nM – open triangles, circles and squares (Δ, ○, □).

Supplementary Fig.S4

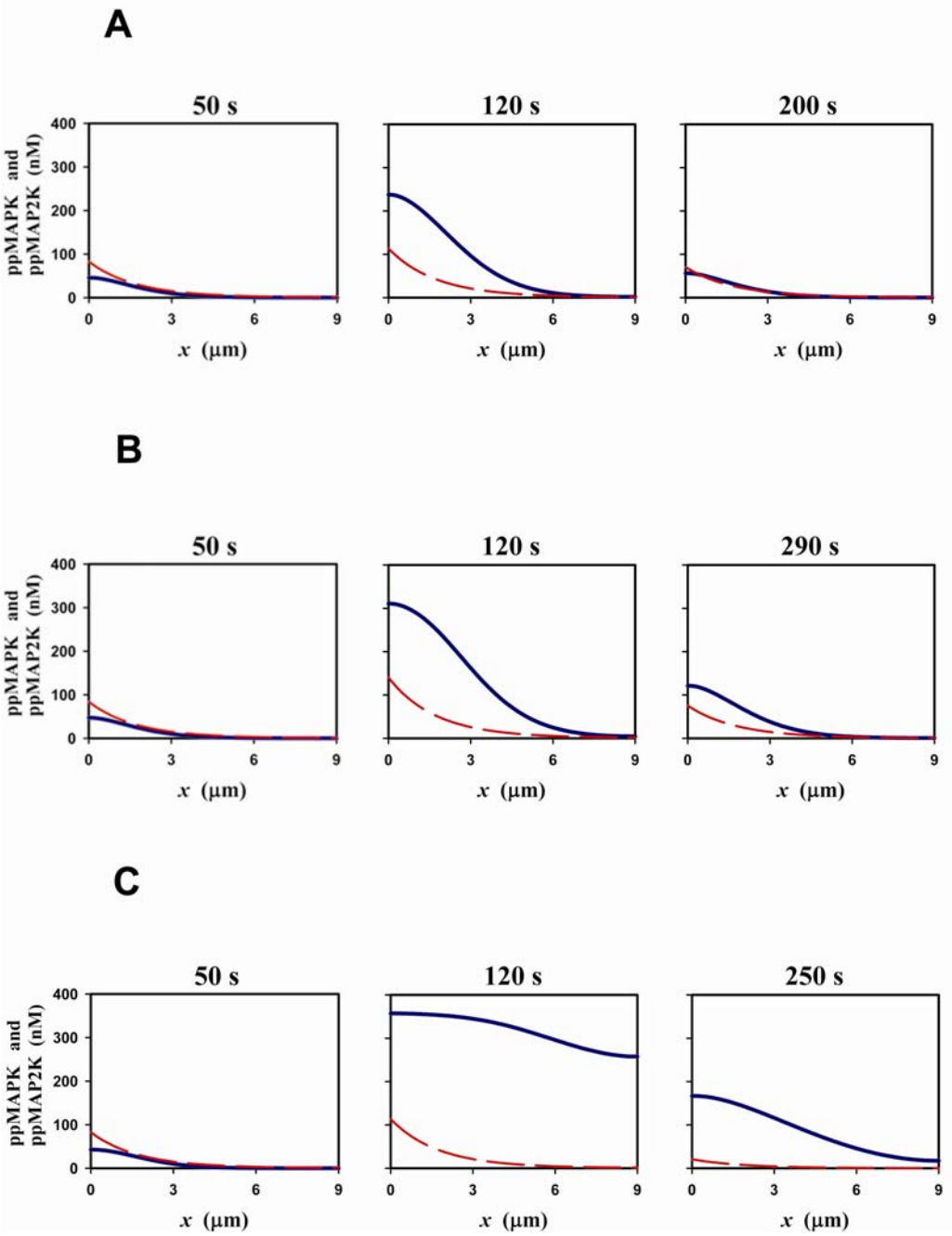

Fig. S4. Spatio-temporal patterns of MAPK activation by a transient stimulus. (A-C) Dynamics of the ppMAPK (solid blue lines) and ppMAP2K (dashed red lines) spatial profiles following the onset of transient Ras activation for three stimulus-response dependencies shown Fig. 1A-C of the main text. The transient time-course of Ras-GTP is described in the legend to Fig. S3; the steady-state levels of Ras-GTP are 5nM. See Tables I-III of the main text for the differential equations and parameters.

The signal propagation pattern can be conveniently scaled using the dimensionless parameter, $\alpha^2 = (L^2 / D)/(K_m^{phosphatase} / V_{\max}^{phosphatase})$, which equals the ratio of the characteristic times of protein diffusion and phosphatase reactions and is recognizable as the Damkohler number (Kholodenko, 2002). Stationary profiles of activated MAPK calculated for different α values (Fig. S5) demonstrate that at given values of protein diffusivity and phosphatase activity, a further increase in the cell size will extend the ppMAPK gradient to a point where the phosphorylated MAPK fraction becomes negligible near the nucleus.

Supplementary Fig. S5.

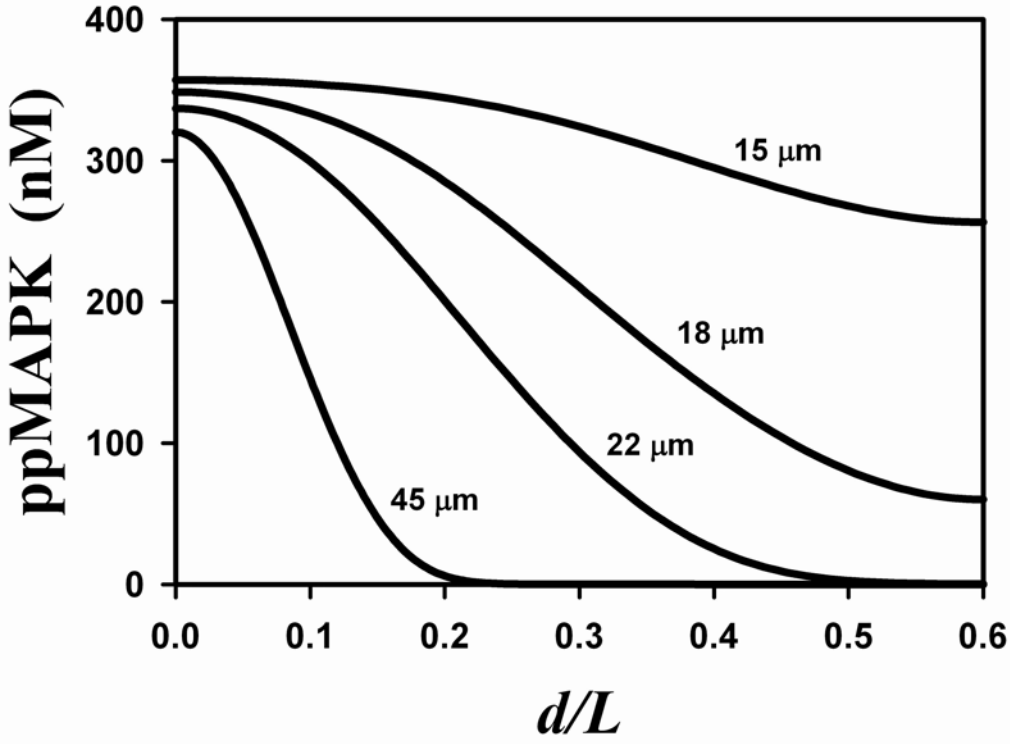

Fig. S5. Steady-state gradients of activated MAPK for various cell sizes. Stationary spatial profiles of MAPK, that crucially depend on the dimensionless parameter (α^2) proportional to the cell size squared (see the text), are presented for bistable MAPK cycle. The cell sizes (radius L = 15, 18, 22, and 45 μm) indicated near the lines correspond to the following values of α^2 = 180, 259.2, 387.2, and 1620, respectively. The spatial coordinate is scaled by the cell size (L), d is the distance from the plasma membrane.

Supplementary Fig. S6

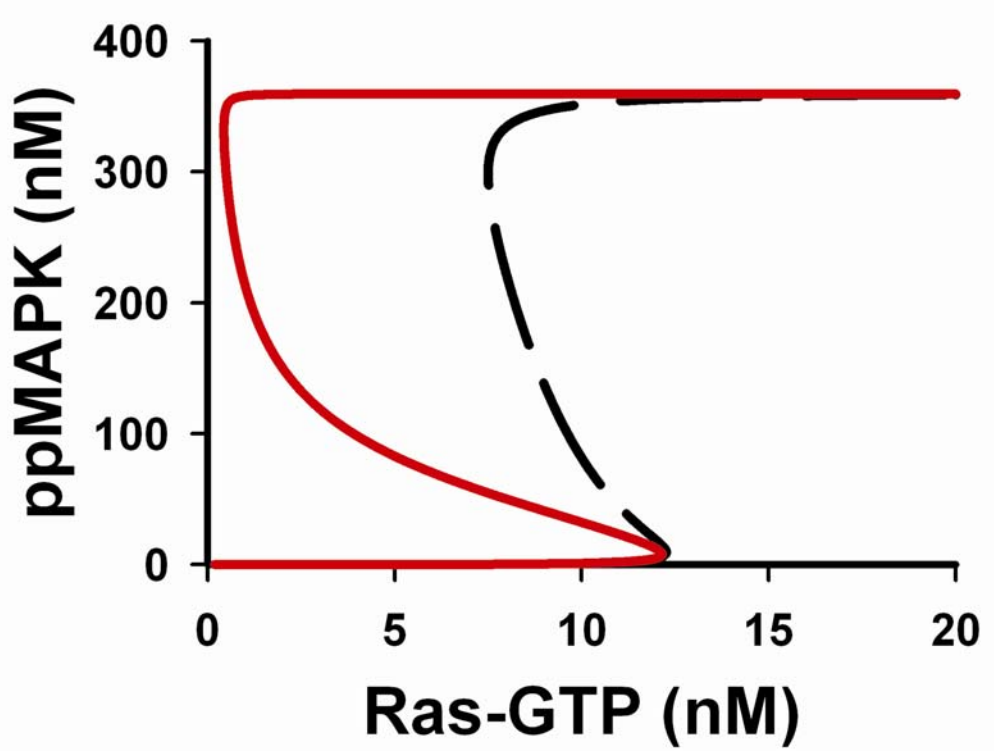

Fig. S6. Input-output relationships of MAPK cascades: Expansion of the bistability range due to MAP2K phosphatase inhibition by active MAPK. The stationary dependences of ppMAPK on Ras-GTP correspond to the bistable ERK cycle and inhibition of the MAP2K phosphatase by ppMAPK (solid red line) or the MAPK cascade without feedback (dashed black line, that is also shown in the insert to Fig. 1C of the main text). The rate equations are given in Tables I-III of the main text and Supplementary Table I.

A possible molecular mechanism to facilitate phosphorelay waves may involve the inhibition of the phosphatases of MAP2K by active MAPK or simply concurrently with MAPK activation, e.g., owing to the production of reactive oxygen species (ROS) triggered by growth factor stimulation. Kinetic description of the inhibition of the phosphatases of MAP2K by active MAPK and ROS are presented in Supplementary Tables I and II, respectively. Most importantly, any of these molecular mechanisms together with MAPK cycle bistability make it possible to propagate the ppMAPK wave over distances of the order of 100 μm (cf. Fig. 3 and Supplementary Fig. S6).

Supplementary Table I.

Kinetic expressions of feedback inhibition of the rates of MAP2K phosphatases by ppMAPK. We assume that feedback inhibition occurs both on the membrane (A) and in the cytosol (B). Inhibition constant, K_i = 70 nM. All the other kinetic parameters are given in Tables II and III in the main text.

A. Cell membrane.

	Reaction	Rate
5	ppMAP2K → pMAP2K	$v_5^m = \dfrac{V_{\max 5}^m \cdot [ppMAP2K]/K_{m5}^m}{(1+([ppMAPK]/K_i)^2)\left(1+[ppMAP2K]/K_{m5}^m+[pMAP2K]/K_{m6}^m+[MAP2K]/K_{i1}^m\right)}$
6	pMAP2K → MAP2K	$v_6^m = \dfrac{V_{\max 6}^m \cdot [ppMAP2K]/K_{m6}^m}{(1+([ppMAPK]/K_i)^2)\left(1+[ppMAP2K]/K_{m5}^m+[pMAP2K]/K_{m6}^m+[MAP2K]/K_{i1}^m\right)}$

B. Cytosol.

	Reaction	Rate
5	ppMAP2K → pMAP2K	$v_5^c = \dfrac{V_{\max 5}^c \cdot [ppMAP2K]/K_{m5}^c}{(1+([ppMAPK]/K_i)^2)\left(1+[ppMAP2K]/K_{m5}^c+[pMAP2K]/K_{m6}^c+[MAP2K]/K_{i1}^c\right)}$
6	pMAP2K → MAP2K	$v_6^c = \dfrac{V_{\max 6}^c \cdot [ppMAP2K]/K_{m6}^c}{(1+([ppMAPK]/K_i)^2)\left(1+[ppMAP2K]/K_{m5}^c+[pMAP2K]/K_{m6}^c+[MAP2K]/K_{i1}^c\right)}$

Supplementary Table II.

Kinetic description of inhibition of phosphatases of the MAPK cascade by ROS.

Inhibition of maximal rates of phosphatases by ROS is assumed to occur both on the membrane and in the cytosol, described by the following expression, $\frac{V_{\max i}\cdot(1+I_0^{\,2})}{(1+(\rho\cdot I_0)^2)}$ (i=2, 5, 6, 9, 10, see Tables II and III in the main text). The dimensionless parameter ρ is the fractional increase in the ROS level relative to the basal level $[ROS]_0$, $\rho = [ROS]/[ROS]_0$; $I_0 = 10$. All the other kinetic parameters are given in Supplementary Tables I and II.

A. Cell membrane.

	Reaction	Rate
2	pMAP3K → MAP3K	$v_2^m = \frac{V_{\max 2}\cdot(1+I_0^{\,2})\cdot[pMAP3K]/K_{m2}}{(1+(\rho\cdot I_0)^2)\cdot\left(1+[pMAP3K]/K_{m2}\right)}$
5	ppMAP2K → pMAP2K	$v_5^m = \frac{V_{\max 5}^m\cdot(1+I_0^{\,2})\cdot[ppMAP2K]/K_{m5}^m}{(1+(\rho\cdot I_0)^2)\left(1+[ppMAP2K]/K_{m5}^m+[pMAP2K]/K_{m6}^m+[MAP2K]/K_{i1}^m\right)}$
6	pMAP2K → MAP2K	$v_6^m = \frac{V_{\max 6}^m\cdot(1+I_0^{\,2})\cdot[ppMAP2K]/K_{m6}^m}{(1+(\rho\cdot I_0)^2)\cdot\left(1+[ppMAP2K]/K_{m5}^m+[pMAP2K]/K_{m6}^m+[MAP2K]/K_{i1}^m\right)}$

B. Cytosol.

	Reaction	Rate
5	ppMAP2K →pMAP2K	$v_5^c = \frac{V_{\max 5}^c\cdot(1+I_0^{\,2})\cdot[ppMAP2K]/K_{m5}^c}{(1+(\rho\cdot I_0)^2)\cdot\left(1+[ppMAP2K]/K_{m5}^c+[pMAP2K]/K_{m6}^c+[MAP2K]/K_{i1}^c\right)}$
6	pMAP2K → MAP2K	$v_6^c = \frac{V_{\max 6}^c\cdot(1+I_0^{\,2})\cdot[ppMAP2K]/K_{m6}^c}{(1+(\rho\cdot I_0)^2)\cdot\left(1+[ppMAP2K]/K_{m5}^c+[pMAP2K]/K_{m6}^c+[MAP2K]/K_{i1}^c\right)}$
9	ppMAPK → pMAPK	$v_9^c = \frac{V_{\max 9}\cdot(1+I_0^{\,2})\cdot[ppMAPK]/K_{m9}}{(1+(\rho\cdot I_0)^2)\cdot\left(1+[ppMAPK]/K_{m9}+[pMAPK]/K_{m10}+[MAPK]/K_{i2}\right)}$
10	pMAPK → MAPK	$v_{10}^c = \frac{V_{\max 10}\cdot(1+I_0^{\,2})\cdot[pMAPK]/K_{m10}}{(1+(\rho\cdot I_0)^2)\cdot\left(1+[ppMAPK]/K_{m9}+[pMAPK]/K_{m10}+[MAPK]/K_{i2}\right)}$

Supplementary Fig. S7.

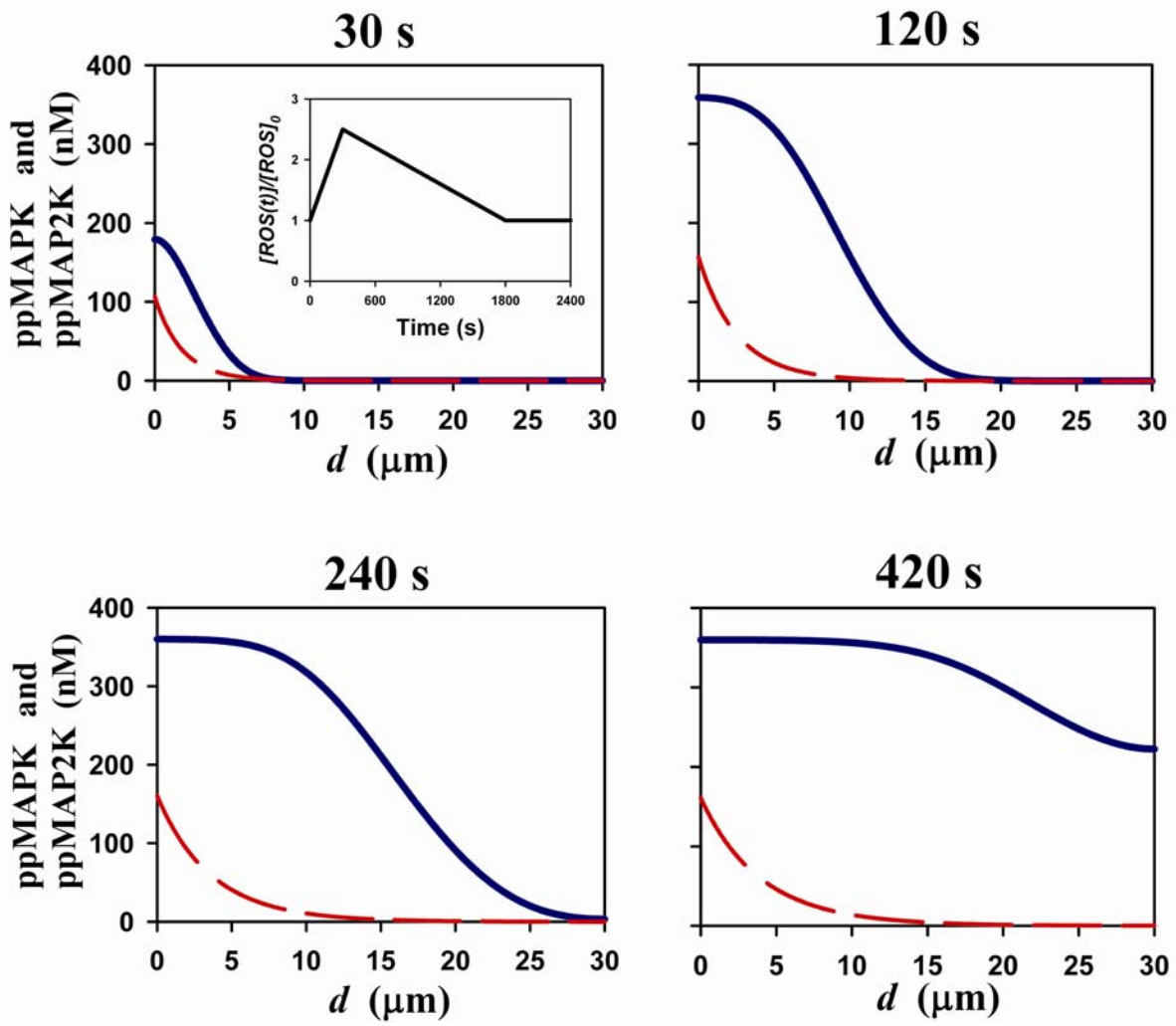

Fig. S7. Phosphorelay waves emerging from bistability in the MAPK cycle and inhibition of the phosphatases by reactive oxygen species (ROS). Snapshots of the ppMAPK wave dynamics following the onset of sustained Ras activation are shown at 30, 120, 240 and 420 seconds. The phosphatases of Raf, MAP2K and MAPK are inhibited by ROS, and the MAPK cycle exhibits hysteresis. The ROS level is reported to increase transiently following growth factor stimulation (Bae et al., 1997; Kim et al., 2003). Based on these experimental data, the time course of the fractional increase in the ROS level ($[ROS]/[ROS]_0$, where $[ROS]_0$ is the basal level) was simulated by the following transient function of time shown in the insert: for $0 < t < t_1 = 300$ s, the initial increase in the ROS level, $[ROS(t)]/[ROS]_0 = 1 + (a-1)\cdot t/t_1$, at $t = t_1 = 300$ s, the peak level $[ROS(t)]/[ROS]_0 = a = 2.5$ is reached. For $t_1 < t < t_2 = 1800$ s, $[ROS(t)]$ descends down to the basal level $[ROS]_0$, as $((1-a)\cdot t + a\cdot t_2 - t_1)/(t_2 - t_1)$, and the basal level is sustained at $t > 1800$ s. Cell radius $L = 50$ μm, nuclear radius M = 20 μm, $D = 2\ \mu m^2 \cdot s^{-1}$, Ras-GTP=30 nM. The rate equations for ROS inhibition of phosphatases are given in Supplementary Table II. All other rate equations are given in Tables I-III of the main text.

Phosphoprotein waves arising from bistability in MAPK cycle feature a spatially inhomogeneous activation threshold, because the ppMAP2K concentration inevitably decreases as the distance from the membrane increases (insert to Fig. 1D in the main text). Interestingly, the fact that signals spread from the cell periphery to the interior where the surface of the wave front decreases facilitates the signal propagation. Figs. S8 and S9 illustrate this space-condensing effect; at the same values of kinetic parameters a one-dimensional wave vanishes at the distance where the wave that travels inside the cell can still deliver the signal.

Supplementary Fig. S8.

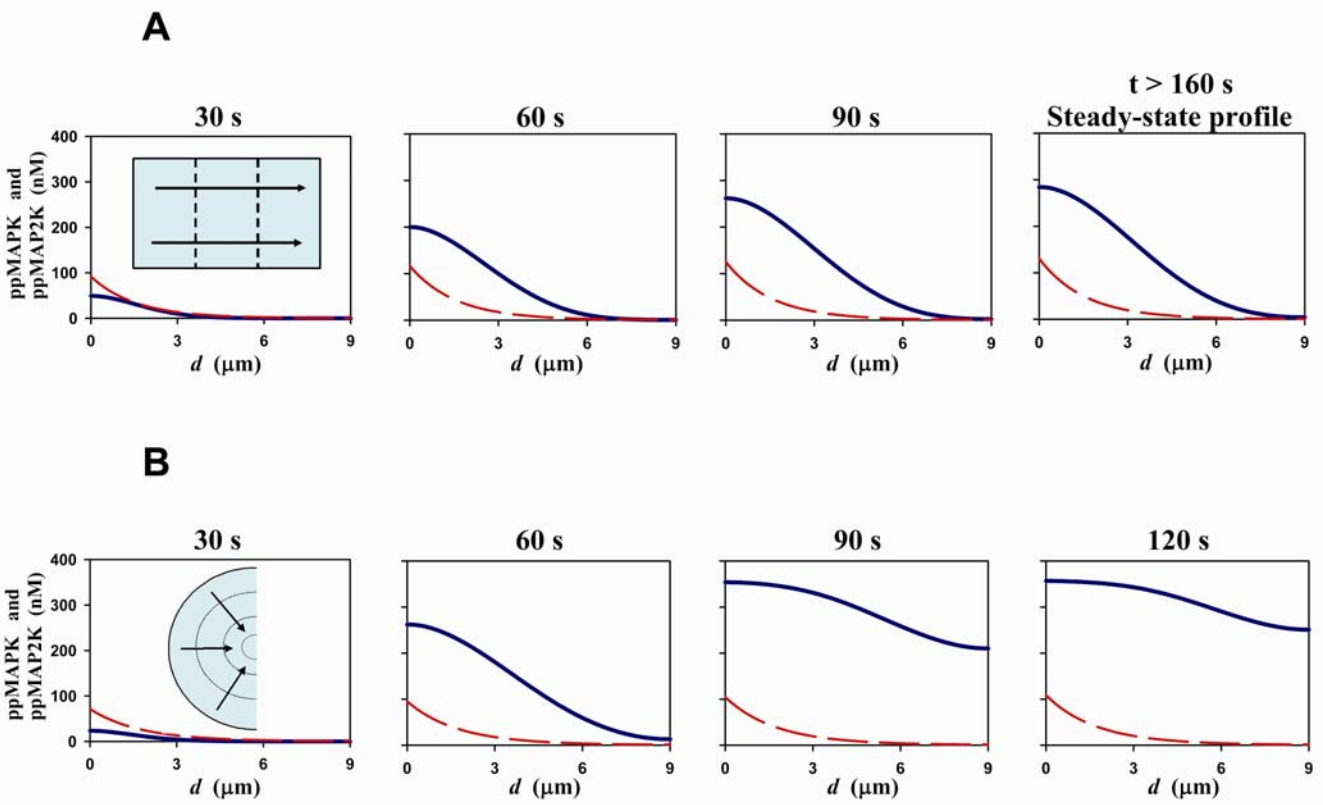

Fig. S8. "Space-condensing" effect facilitates the wave propagation from the plasma membrane to the cell center. Propagation of phosphoprotein waves in one dimension (**A**) and from the plasma membrane to the center of a spherical cell (**B**). Waves emerge from bistability in the MAPK cycle and the wave solutions are calculated at the same values of kinetic parameters and diffusivity. Solid (blue) line and dashed (red) lines correspond to ppMAPK and ppMAP2K, respectively. (**B**). Cell radius L = 15 μm, nucleus radius Q = 6 μm. The kinetic parameters are the same as in Fig. 1C.

Supplementary Fig. S9.

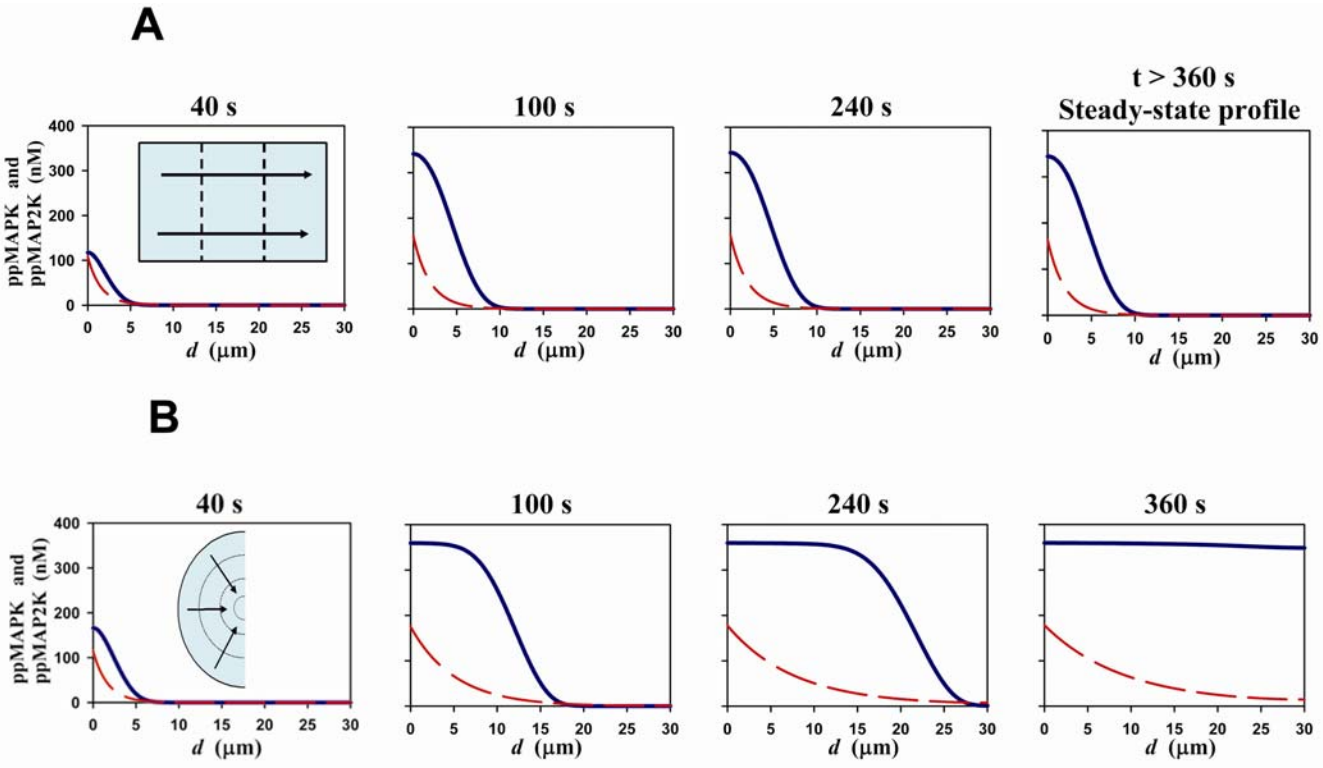

Fig. S9. Propagation of phosphoprotein waves facilitated by feedback inhibition of MAP2K phosphatase in one dimension (A) and from the membrane to the center of a spherical cell (B). Waves emerge from feedback inhibition of MAP2K phosphatase and bistability in the MAPK cycle and are calculated at the same values of kinetic parameters and diffusivity ($D = 2\ \mu m^2 \cdot s^{-1}$). The rate equations and the kinetic and space parameters are the same as in Fig. 2 of the main text.

Signaling via phosphoprotein waves has key advantages over solely diffusive signal propagation. Fig. 3 of the main text demonstrates that short positive feedback in the cytoplasm (see Supplementary Table III) enables protein kinase/phosphatase cascades to transmit phosphorylation signals over much longer distances than 100 μm.

Supplementary Table III.
Kinetic description of a short positive feedback from MAPK to MAP2K.

Activation of MAP2K by active MAPK is mediated by a cytoplasmic kinase that has a negligible activity ($10^{-5} \cdot V_{max}$) in the absence of activated MAPK ([ppMAPK] = 0). In simulations presented in Fig 7 of the main text, the dimensionless parameter G_a=20.

	Reaction	Rate	Kinetic constants
3	MAP2K → pMAP2K	$v_3^c = \frac{V_{\max 3}^c \cdot [MAP2K]/K_{m3}}{(1+[MAP2K]/K_{m3}+[pMAP2K]/K_{m4})} \cdot \frac{(10^{-5}+G_a \cdot ([ppMAPK]/K_a)^2)}{(1+([ppMAPK]/K_a)^2)}$	$V_{\max 3}^c$ =1 μM·s^{-1} K_{m3} =130 nM K_a=10 nM
4	pMAP2K → ppMAP2K	$v_4^c = \frac{V_{\max 4}^c \cdot [pMAP2K]/K_{m4}}{(1+[MAP2K]/K_{m3}+[pMAP2K]/K_{m4})} \cdot \frac{(10^{-5}+G_a \cdot ([ppMAPK]/K_a)^2)}{(1+([ppMAPK]/K_a)^2)}$	$V_{\max 4}^c$ =1 μM·s^{-1} K_{m4} =50 nM

Supplementary Fig. S10 illustrates that the velocity of the wave increases with the strength of short positive feedback (see Supplementary Table III).

Supplementary Fig. S10.

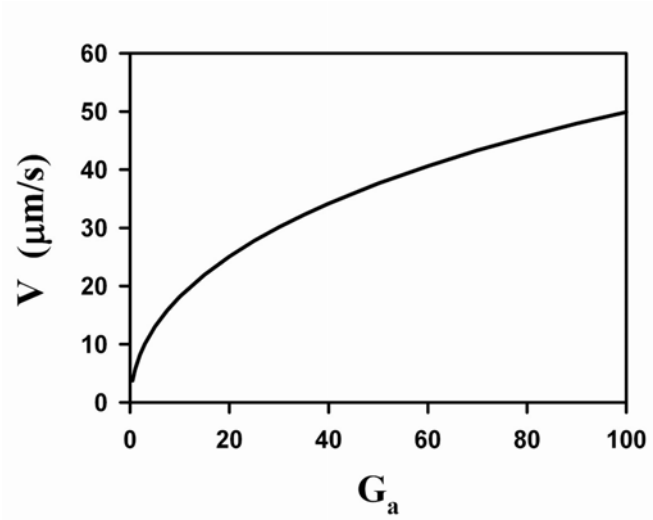

Fig. S10. Dependence of the velocity of the ppMAPK traveling wave on the strength of the feedback from MAPK to MAP2K. Waves emerge from feedback activation of MAP2K by ppMAPK and bistability in the MAPK cycle. The rate equations and the kinetic and space parameters are the same as in Fig. 3 of the main text. An increase in the dimensionless parameter G_a enhances the strength of the positive feedback from MAPK to MAP2K (described in Supplementary Table III).

Numerical Methods

Numerical integration of the reaction-diffusion system presented in Table 1 will first be illustrated for one-dimensional spatial domain, $0 \le x \le L$, using the following equation (1) and the initial condition (2):

$$\frac{\partial u}{\partial t} = f(x,t) + D\frac{\partial^2 u}{\partial x^2}, \qquad 0 \le x \le L \qquad (1)$$

$$u(x,0) = u_0(x), \quad x \in [0,L] \qquad (2)$$

We will consider two types of the boundary conditions, Eq. 3a corresponding to impermeable boundaries (see Table 1 for [*pMAPK*] and [*ppMAPK*]), and Eq. 3b corresponding to the reactions at the surface (see flux boundary conditions in Table 1 of the main text for [*pMAP2K*] and [*ppMAP2K*]),

$$\frac{\partial u}{\partial x}\Big|_{x=0,L} = 0 \qquad (3a)$$

$$\frac{\partial u}{\partial x}\Big|_{x=L} = g(u) \qquad (3b)$$

To solve this problem numerically, the partial derivatives are replaced by finite differences,

$$\frac{\partial u(x,t)}{\partial t} \approx \frac{u(x,t+\tau) - u(x,t)}{\tau}, \qquad \frac{\partial^2 u(x,t)}{\partial x^2} \approx \frac{u(x+h,t) - 2u(x,t) + u(x-h,t)}{h^2}. \qquad (4)$$

The time and space are discretized on the mesh, $\{x_m, t_n\}$, $m=0,1,\ldots,M$, $n=0,1,2,\ldots$. We used $x_m = mh$, $h = L/M$; $t_n = n\tau$, where h and τ are the space and time steps, respectively. The approximate value of the solution $u(x, t)$ at each grid point (x_m, t_n) is denoted by $u_m^n \approx u(x_m, t_n)$. The finite-difference scheme has the form,

$$\frac{u_m^{n+1} - u_m^n}{\tau} = D\frac{u_{m+1}^n - 2u_m^n + u_{m-1}^n}{h^2} + f_m^n. \qquad (5)$$

After a re-arrangement we obtain,

$$u_m^{n+1} = u_m^n + \frac{\tau D}{h^2}(u_{m+1}^n - 2u_m^n + u_{m-1}^n) + \tau f_m^n, \qquad \text{m} = 1,2,\ldots,\text{M-1}. \qquad (6)$$

The boundary conditions given by Eqs. 3a and 3b correspond to the following Eqs. 7a and 7b, respectively,

$$u_0^{n+1} = u_1^{n+1}, \quad u_M^{n+1} = u_{M-1}^{n+1} \qquad (7a)$$

$$u_M^{n+1} = u_{M-1}^{n+1} + hg(u_M^n) \qquad (7b)$$

Spherical symmetry makes the analysis of signaling in three dimensions nearly equivalent to the analysis in one dimension. The Laplacian in 3D has the form, $\Delta u = \frac{\partial^2 u}{\partial x^2} + \frac{\partial^2 u}{\partial y^2} + \frac{\partial^2 u}{\partial z^2}$. In the case of full spherical symmetry, the Laplace operator takes the form, $\Delta u = \frac{1}{\rho^2}\frac{\partial}{\partial \rho}\left(\rho^2 \frac{\partial u}{\partial \rho}\right)$, where ρ is the distance from the cell center. For a spherical cell, Eq. 1 takes the following form,

$$\frac{\partial u}{\partial t} = f(\rho,t) + D\frac{\partial^2 u}{\partial \rho^2} + \frac{2D}{\rho}\frac{\partial u}{\partial \rho} = f(\rho,t) + \frac{D}{\rho^2}\frac{\partial}{\partial \rho}\left(\rho^2 \frac{\partial u}{\partial \rho}\right) \qquad (8)$$

with the following boundary conditions at the impermeable boundaries (see boundary conditions in Table 1 of the main text for [*pMAPK*] and [*ppMAPK*]):

$$\frac{\partial u}{\partial \rho}\Big|_{\rho=Q,L} = 0 \qquad (9a)$$

and the following flux conditions (see Table 1 for [*pMAP2K*] and [*ppMAP2K*]),

$$\frac{\partial u}{\partial \rho}\Big|_{\rho=L} = g(u) \qquad (9b)$$

where L is the cell radius, and Q is the nuclear radius.

For Eq. 9, the finite-difference scheme with $x_m = mh$, $h = (L-Q)/M$; $t_n = n\tau$, ($m=0,1,\ldots,M$, $n=0,1,2,\ldots$) has the following form,

$$u_m^{n+1} = u_m^n + \frac{\tau D}{h^2}(u_{m+1}^n - 2u_m^n + u_{m-1}^n) + \frac{\tau D}{mh}\frac{(u_{m+1}^n - u_{m-1}^n)}{h} + \tau f_m^n \quad m = 1,2,\ldots,M\text{-}1. \quad (10)$$

For calculations we used dimensional units. We selected the M value that corresponded to $h = 0.1$ μm; we used $\tau = 0.001$ s.

The [*pMAP2K*] and [*ppMAP2K*] values at the boundary $\rho = L$ (*for* $m = M$) were found by solving the following system of two algebraic equations,

$$\begin{aligned} u_{1,M}^{n+1} &= u_{1,M-1}^{n+1} + hg_1(u_{1,M}^{n+1}, u_{2,M}^{n+1}) \\ u_{2,M}^{n+1} &= u_{2,M-1}^{n+1} + hg_2(u_{1,M}^{n+1}, u_{2,M}^{n+1}) \end{aligned} \qquad (11)$$

Here, $u_{1,m}$ is [*pMAP2K*], $u_{2,m}$ is [*ppMAP2K*] (the values at $m = M$-1 are assumed to be already calculated using Eq. 10), and the functions g_1 and g_2 are determined as follows,

$$g_1 = \frac{L}{3D}(v_3^{mem} - v_4^{mem} + v_5^{mem} - v_6^{mem})$$
$$g_2 = \frac{L}{3D}(v_4^{mem} - v_5^{mem}) \qquad (12)$$

Here the reactions rates v_i^{mem} are functions of the variables [*pMAP2K*] and [*ppMAP2K*] (presented in Table 2; note that in Table 1 these functions are multiplied by a factor $L^2/3D$, because the dimensionless variable $x = \rho/L$ was used). The solution to Eq. 11 was found by Newton's iteration method.

References

Asthagiri, A.R. and Lauffenburger, D.A. (2001) A computational study of feedback effects on signal dynamics in a mitogen-activated protein kinase (MAPK) pathway model. *Biotechnol Prog*, 17, 227-239.

Bae, Y.S., Kang, S.W., Seo, M.S., Baines, I.C., Tekle, E., Chock, P.B. and Rhee, S.G. (1997) Epidermal growth factor (EGF)-induced generation of hydrogen peroxide. Role in EGF receptor-mediated tyrosine phosphorylation. *J Biol Chem*, 272, 217-221.

Chiloeches, A., Paterson, H.F., Marais, R., Clerk, A., Marshall, C.J. and Sugden, P.H. (1999) Regulation of Ras.GTP loading and Ras-Raf association in neonatal rat ventricular myocytes by G protein-coupled receptor agonists and phorbol ester. Activation of the extracellular signal-regulated kinase cascade by phorbol ester is mediated by Ras. *J Biol Chem*, 274, 19762-19770.

Huang, C.Y. and Ferrell, J.E., Jr. (1996) Ultrasensitivity in the mitogen-activated protein kinase cascade. *Proc Natl Acad Sci U S A*, 93, 10078-10083.

Kholodenko, B.N. (2000) Negative feedback and ultrasensitivity can bring about oscillations in the mitogen-activated protein kinase cascades. *Eur J Biochem*, 267, 1583-1588.

Kholodenko, B.N. (2002) MAP kinase cascade signaling and endocytic trafficking: a marriage of convenience? *Trends Cell Biol*, 12, 173-177.

Kim, H.S., Song, M.C., Kwak, I.H., Park, T.J. and Lim, I.K. (2003) Constitutive induction of p-Erk1/2 accompanied by reduced activities of protein phosphatases 1 and 2A and MKP3 due to reactive oxygen species during cellular senescence. *J Biol Chem*, 278, 37497-37510.

Maly, I.V., Wiley, H.S. and Lauffenburger, D.A. (2004) Self-organization of polarized cell signaling via autocrine circuits: computational model analysis. *Biophys J*, 86, 10-22.

Markevich, N.I., Hoek, J.B. and Kholodenko, B.N. (2004a) Signaling switches and bistability arising from multisite phosphorylation in protein kinase cascades. *J Cell Biol*, 164, 353-359.

Markevich, N.I., Moehren, G., Demin, O., Kiyatkin, A., Hoek, J.B. and Kholodenko, B.N. (2004b) Signal processing at the Ras circuit: What shapes Ras activation patterns? *IEE Systems Biology*, 1, 104-113.